PHYSICAL REVIEW B VOLUME 35, NUMBER 5 15 FEBRUARY 1987-I

Site-selective laser spectroscopy of defect aggregation kinetics in KCl:Sm^{2+}

A. J. Ramponi* and J. C. Wright
Department of Chemistry, University of Wisconsin, Madison, Wisconsin 53706
(Received 2 September 1986)

The mechanism for the aggregation kinetics of alkali halides doped with divalent cations has received considerable attention. However, controversy still exists over whether the initial aggregation involves dimer or trimer formation. Site-selective laser experiments have been performed to follow the concentration changes of all the sites simultaneously during the aggregation process. The concentration dependence of the rate constant for the growth of the dominant cluster site shows that the aggregation follows second-order kinetics and the cluster site is a dimer. The spectroscopic transitions of the two ions within the dimer are identified and shown to arise from two crystallographically inequivalent sites. Higher-order clusters form at longer times. There is also a number of minor sites that are dependent upon the individual crystal samples. The quenching procedures commonly used for dissociating the clusters are found to be less effective than previously assumed since an appreciable number of clusters is still present in the spectrum immediately following the quench.

I. INTRODUCTION

The aggregation of divalent cation impurities in alkali halide crystals has served as a model for the dynamics of defect aggregation in solid-state chemistry. The divalent cation enters the alkali halide lattice substitutionally in place of a host cation while a cation vacancy is created for charge compensation. The divalent impurities and cation vacancies can be present in the lattice as free divalent ions and free vacancies, associated in pairs to form impurity-vacancy (IV) dipoles, or associated as clusters consisting of two or more IV pairs. Many investigations have been performed on the aggregation of IV pairs, yet the nature of the clusters and the order of the kinetics involved in their formation are still in doubt. The experimental approach involves heating the crystal to a high enough temperature so that virtually all the clusters are broken apart leaving only single-pair IV dipoles. The crystal is then rapidly quenched to ensure that the site distribution characteristic of the elevated temperature is preserved. If after this procedure the crystal is annealed at a constant temperature, typically between room temperature and 100 °C, the initial concentration of dipoles is observed to decline while clusters such as dimers (two IV pairs) and trimers (three IV pairs) begin to reform. Cook and Dryden[1,2] were the first to investigate the kinetics of dipole aggregation for a variety of divalent cations in NaCl and KCl crystals. It was observed that the aggregation proceeds in two stages separated by a plateau region from which the second stage of aggregation proceeds much more slowly. During the first stage of aggregation, dipole decay occurs relatively quickly up to the plateau and the rate of disappearance of dipoles is proportional to the third power of the dipole concentration. They also show that the concentration dependence of the rate constant is consistent with a third-order reaction. Third-order kinetics implies that the first stage of aggregation results from the direct formation of a trimeric cluster consisting of three IV dipoles. This observation was surprising since pure third-order reactions are extremely rare and the random encounter of three dipoles is far less probable than the encounter of two dipoles to form a dimer.[3] Cook and Dryden further concluded that the plateau region between the two stages of aggregation represents an equilibrium between free dipoles and trimers. The segment of the decay curve for which the plateau occurs was shown to be dependent on the annealing temperature and the initial impurity concentration. It was also hypothesized that the second stage of aggregation, beyond the plateau, represents the formation of higher-order clusters created from trimers and the remaining dipoles.

As an alternative to the third-order reaction, Crawford[4] suggested that the third-order kinetics could be explained if two dipoles associate to form a loosely coupled dimer which in turn captures a third dipole to form a trimer. If the loosely bound dimer retains a residual dipole moment and exists in quasiequilibrium with the free dipoles, then dipole decay would still appear to follow third-order kinetics. Unger and Perlman[5] performed experiments similar to those of Cook and Dryden and concluded that the initial stage of aggregation instead follows pure second-order kinetics with correction for the dissociation or back reaction of the dimers. The disagreement between the interpretations was not resolved in subsequent exchanges[6,7] where Cook and Dryden pointed out that the concentration dependence of the rate constants was the parameter that defined the reaction order.[6]

Computer simulations were performed by Dienes to study the kinetics of dipole clustering in alkali halides.[8] His simulations predict that at high dopant levels, third-order kinetics suitably describes the dipole decay curve independently of the initial concentration but at low dopant levels second-order kinetics dominates the initial decay with the derived rate constants dependent on the initial concentration. At intermediate concentrations, third-order kinetics dominate at early times while second-order

kinetics adequately fit the decay curve for longer times. From these results Dienes concludes that it is necessary to study several systems over a wide range of annealing temperatures and concentrations in order to reach a self-consistent reaction kinetics theory. In yet another simulation, Lilley[9] used the Unger-Perlman model[5] to show that one cannot distinguish between dimer and trimer solely on the basis of the decay curve shape. He proposed a dimer-trimer model[10] similar to Crawford's[4] where the concentration of dimers which form as precursors to trimers is so small that the overall kinetics appear to be third order.

More recently, Rubio and co-workers[11] performed a thorough investigation of the aggregation kinetics for europium-doped alkali halide crystals. The dipole decay curves were analyzed in terms of both pure second- (Unger-Perlman model) and pure third-order kinetics with back reaction. Their results indicate that both models describe the decay curves to the same degree of accuracy, supporting Lilley's[9] assertion that the Unger-Perlman model cannot distinguish between dimer and trimer formation. The ambiguity was removed by studying the concentration dependence of the rate constant at the start of aggregation where clustering was small and the back reaction could be neglected. The approach paralleled that of Cook and Dryden.[1,2,6] The analysis showed that the aggregation occurred by second-order kinetics and they concluded that dimers are the complexes formed during the initial stage of aggregation. Munoz, Galo, Patron, and Rubio[12] have since performed similar experiments on manganese-doped NaCl and KCl where the dimers were also seen as the first cluster to form during the initial stage of aggregation.

In this paper, we present the application of site-selective laser spectroscopy to the study of aggregation kinetics in KCl:Sm^{2+}. The narrow f-f transitions characteristic of charge-compensated divalent samarium in the alkali halide host offer a convenient method for directly monitoring the different sites and precipitated phases. Another advantage in selecting this system is that only one single-pair site with $C_{2v}[110]$ symmetry results from the high-temperature anneal-quench procedure so cluster formation must originate from only one type of dipole. This center is labeled site a in a previous publication. In addition, there are eight sites identified with clusters labeled b, c, d, g, i, j, k, and ϵ.[13] Since each center possesses a unique optical transition in the $^7F_0 \rightarrow {}^5D_0$ excitation spectrum, the evolution of the cluster sites beginning from the high-temperature quench can be reliably followed as a function of sample annealing. The spectra observed immediately following the high-temperature anneal-quench procedure show that the cluster sites, although markedly reduced in relative concentration compared to the single-pair site, are not eliminated as is commonly assumed.[11] A line associated with a cluster that has been labeled g/k is the dominant aggregation product for all the crystals investigated. This line is the result of spectral overlap in the $^7F_0 \rightarrow {}^5D_0$ spectrum between sites g and k.[13] The individual sites were determined from high-resolution $^5D_0 \rightarrow {}^7F_1$ fluorescence spectra to have the same rate of reappearance. New sites that depend on the initial dopant concentration also appear weakly in the quenched samples. However, these sites show very little change in relative concentration over the annealing period, suggesting they are unimportant in determining the overall reaction mechanism. The kinetics of the g/k site formation and the $C_{2v}[110]$ site decay could be described equally well by second- and third-order kinetics with correction for back reaction. The concentration dependence of the rate constant, however, showed that the growth curves are a second-order process in agreement with the findings by Rubio and co-workers.[11]

II. EXPERIMENTAL METHODS

A detailed description of the site-selective laser method and apparatus has been given elsewhere.[14] The laser experiments were performed at 4.2 K. Dye laser intensity and gain profile were monitored over the course of an experiment using a p-i-n photodiode. Excitation spectra were obtained with a low-resolution 0.25-m Fastie-Ebert monochromator to simultaneously monitor fluorescence from all sites. Single-site fluorescence spectra were measured with a high-resolution 1-m Czerny-Turner monochromator. The fluorescence was detected by a gated RC integrator. Conventional absorption spectra using a 200-W tungsten-iodine lamp were measured at 12 K to monitor absolute changes in the dipole concentration.

The crystals were grown from a molten mixture of $SmCl_3$ and KCl by the Czochralski method.[15] The partitioning of Sm^{2+} in KCl is unfavorable and much larger Sm concentrations were present in the melt than were observed in the final crystals. The determination of Sm concentration in the crystals is a crucial step in an experiment directed toward determining the order of the aggregation reaction. Three methods were used to measure the concentrations of Sm in the actual crystals used in the experiment. Neutron activation analysis was used to measure the total Sm concentration in the crystals after the experiments were completed. The absorption strength of the strong $4f^6 \rightarrow 4f^5 5d^1$ interconfigurational absorption band of Sm^{2+} was also measured at room temperature and compared to a crystal with a known dopant concentration, as measured by neutron activation analysis. Finally, the integrated absorption strength of the $^7F_0 \rightarrow {}^5D_1$ absorption line for site a was measured in each of the crystals that had been quenched from high temperature, so the site a concentration was a maximum. The first method measures the total Sm concentration in all its forms regardless of phase or valence state. This method of measuring the Sm concentration participating in the aggregation kinetics will lead to erroneous results if there are inclusions or other microscopic domains of Sm that do not contribute to the aggregation process. The second method measures all of the Sm^{2+} in all of the sites and phases present. The accuracy of this approach is dependent upon the relative absorption strengths of the Sm^{2+} absorption band for each of the different sites and the relative number of different sites. In our case, the Sm^{2+} is dominantly in the $C_{2v}[110]$ site after the crystals were quenched and there should be little error associated with the measurement. The third method measures only the Sm^{2+} in site a, the actual site involved in the aggregation kinetics. This measurement is the most direct determination of the concen-

tration actually involved in the equilibrium but it does not include the concentrations of the cluster sites that are present after the crystals are quenched. The ratios of the crystal concentrations measured by neutron activation analysis were 1:1.4:4.0:5.3, by room-temperature absorption of the $4f^6 \rightarrow 4f^5\,5d^1$ band 1:2.4:8.1:11.0, and by low-temperature absorption of the a site $^7F_0 \rightarrow {}^5D_1$ transition 1:2.2:8.9:11.7. There were large variations in the total Sm concentration measured by neutron activation analysis within any one boule. Thus different crystals or even different portions of a crystal from the same sample boule could have quite different total Sm concentrations. On the other hand, the spectroscopic measurements do not show such variations. Evidently, a small amount of the Sm dopant enters the lattice homogeneously as Sm^{2+}, while the remainder of the Sm remains suspended inhomogeneously throughout the crystal boule. The two spectroscopic measurements are in good agreement with each other and are the most direct measurement of the Sm^{2+} actually available for the aggregation. The concentrations quoted in the text are the result of the second measurement method.

Two methods were used to quench the crystals from high temperatures. In the first, the crystals were encapsulated in quartz tubes under a vacuum of 5×10^{-6} Torr, heated to either 500 or 650 °C for 24 h and quenched by direct immersion of the tube in ice water. Site-selective laser measurements showed that clusters were still present, contrary to accepted views. In order to achieve the fastest possible quenching rate, a second method was devised. The crystals were placed inside a spiraled platinum wire cage and inserted into a long quartz tube. The tube was open at both ends and a large dimple located at approximately one-third the tube's length from the bottom served as a ledge, preventing the crystals from falling through the quartz tube. The tube and samples were positioned within a tube furnace mounted at a 45° angle. A flow of nitrogen gas was continuously passed over the crystals and a thermocouple monitored the furnace temperature. Quenching was accomplished by rotating the quartz tube until the samples were forced off the dimple causing them to fall through the tube and into a Dewar of liquid nitrogen (−196 °C). Crystals treated by this procedure were annealed at approximately 550 °C for 3 h before quenching. Even under these quenching conditions cluster sites were still observed in the spectrum at approximately the same relative concentration as measured in the crystals quenched by the first method.

The annealing experiments were performed by heating a crystal for a given time after it had been quenched from a high temperature, removing it for measurement at low temperatures and returning it for further annealing. The low-temperature annealing treatments were performed in air using a large drying oven. Temperatures were determined to be stable to ±1 °C for temperatures in the range from 40 to 200 °C. Both the low-resolution $^7F_0 \rightarrow {}^5D_0$ excitation spectrum and the broad-band absorption spectrum of the $^5D_1$ level were obtained immediately following the high-temperature anneal-quench procedure and remeasured after each low-temperature anneal. The crystals were stored under liquid nitrogen to ensure that reaggregation of the dipoles did not occur during the time interval between consecutive annealing treatments.

III. RESULTS AND DISCUSSION

A. Kinetics of site distribution

The site-selective laser spectroscopy of KCl:Sm^{2+} has been discussed in a previous paper.[14] The excitation spectrum for the $^7F_0 \rightarrow {}^5D_0$ transition monitoring fluorescence at 726.5 nm with a low-resolution 0.25-m monochromator affords a convenient means of simultaneously observing all the charge-compensated sites. Figure 1 shows the

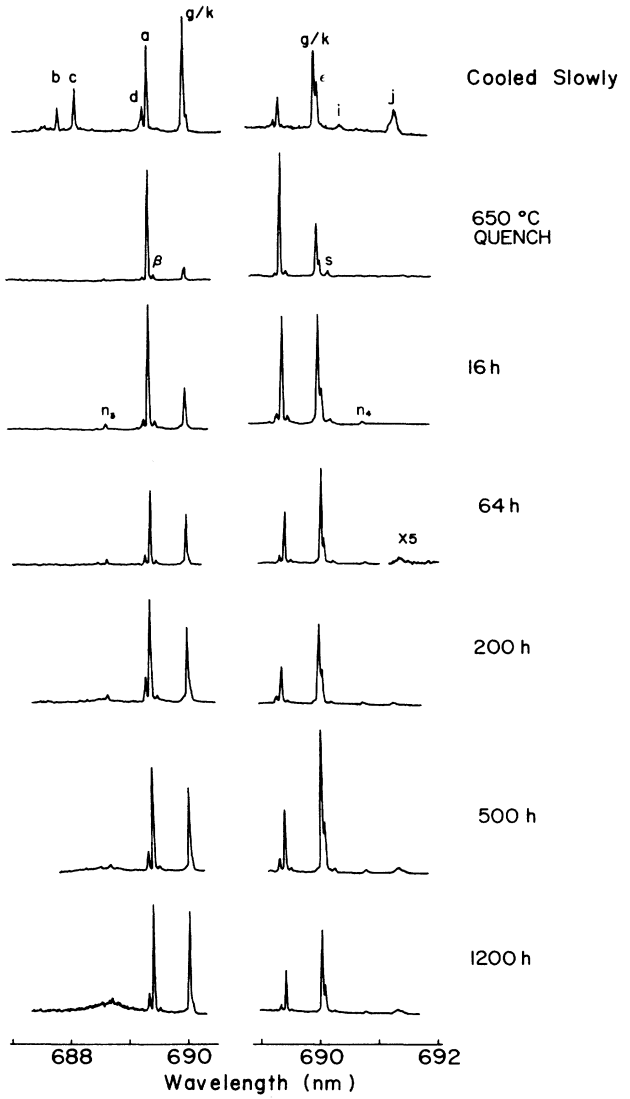

FIG. 1. $^7F_0 \rightarrow {}^5D_0$ excitation spectrum monitoring fluorescence from all sites at 726.5 nm for the 89-ppm crystal. The left column corresponds to a delay of 200 μs and gate of 1 ms; the right column to a delay of 40 μs and gate of 1 ms. The top two rows show the changes in the site distribution that result from the high-temperature anneal-quench procedure. The remaining spectra represent a sampling of the spectral changes resulting from annealing the same crystal at 50 °C for progressively longer times.

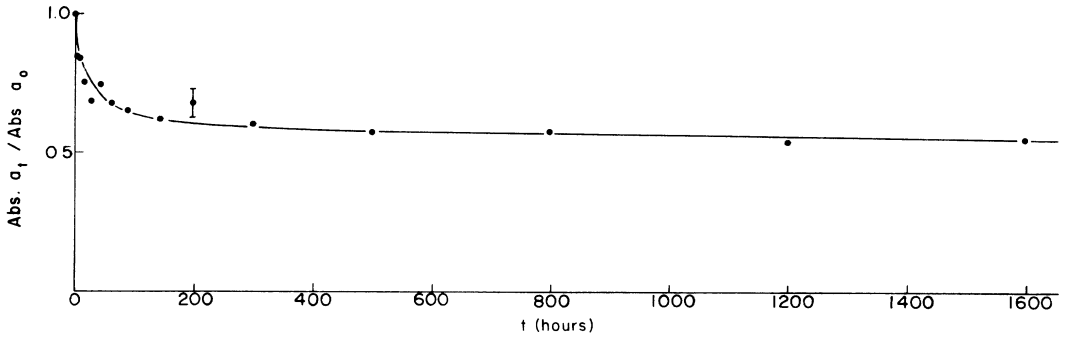

FIG. 2. Relative decay in dipole concentration for the 89-ppm crystal annealed at 50 °C. The curve is to guide the eye.

changes that occur in the site distribution as a result of the high-temperature anneal-quench procedure and subsequent low-temperature annealing at 50 °C for a KCl:Sm^{2+} crystal with 89 ppm Sm^{2+} concentration. Each line in the spectrum corresponds to a unique crystallographic center because the $^7F_0 \rightarrow {}^5D_0$ transition can have only one line per site. The line labeled g/k represents two distinct sites which have overlapping $^7F_0 \rightarrow {}^5D_0$ transitions. The excitation spectra were obtained at 4.2 K due to the strong temperature-dependent fluorescence quenching of sites a and k.[13] The left and right columns correspond to spectra collected for different delay times for the gated integrator of 200 and 40 μs, respectively. The shorter delay times accentuate the clusters which have rapid fluorescence decays. The top spectra show the site distribution observed in the crystals prior to any heat treatment. The spectral characteristics for each of the sites have been described in Ref. 13. Site a was shown to be a single-pair site with $C_{2v}[110]$ symmetry. The other sites correspond to clusters which can be sharply reduced by quenching from elevated temperatures as shown in Fig. 1. However several new sites (labeled β, s, n_3, and n_4) appear weakly as a result of the quench. They have only small variations in intensity (with the exception of site β to be discussed below) even for the longest anneal times. Sites b and c, which were present in the original crystal but completely eliminated by the high-temperature quench, have failed to reappear after 1600 h of crystal annealing. On the other hand, site g/k is observed to undergo marked changes with anneal time relative to the other sites. The broad

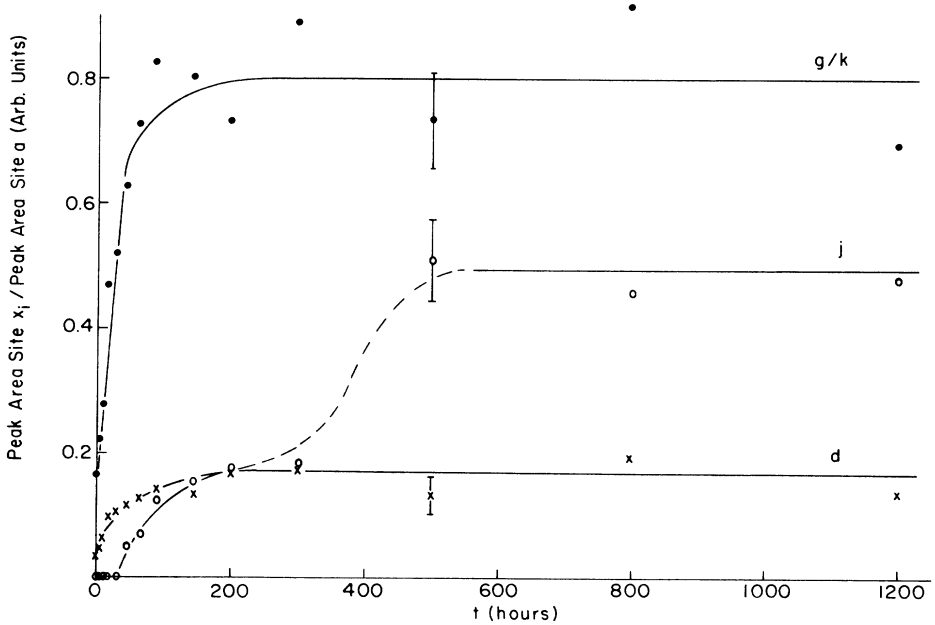

FIG. 3. Growth curves for sites g/k (689.85 nm), d (689.10 nm), and j (691.27) relative to site a for the 89-ppm crystal annealed at 50 °C. The growth curves for sites g/k and d were determined from excitation spectra measured with a delay of 200 μs and gate of 1 ms. The site g/k and site d ratios in the unannealed sample are 1.03 and 0.23, respectively. The growth curve for site j was determined from excitation spectra measured with a delay of 40 μs and gate of 1 ms. The ratio corresponding to the unannealed sample is 1.76. The curves are to guide the eye.

SITE	LIFETIME (ms) 2.2 K	4.2	12
a	10.58	10.60	7.86
k	5.99	0.156	QUENCHED
g	—	0.150	≤0.01

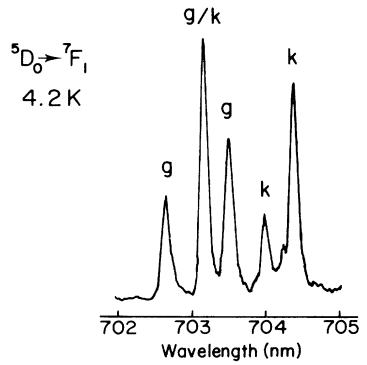

FIG. 4. High-resolution $^5D_0 \rightarrow ^7F_1$ fluorescence spectrum for site g/k exciting the $^5D_0$ level at 689.85 nm. Fluorescence lifetimes of the $^5D_0$ level are also shown for sites a, k, and g for different temperatures. The intensity of site g relative to site k at 2.2 K is too weak to reliably determine the lifetime.

fluorescence centered around 688.70 nm beginning to appear after approximately 200 h of annealing is thought to represent a large cluster that may be related to the formation of a Suzuki phase.[16]

Absolute changes in the dipole concentration (site a) are followed by measuring the absorption spectrum of the $^5D_1$ level after each annealing treatment. The integrated area of the strong absorption located at 636.90 nm in the $^5D_1$ level is used to monitor the decay of site a (see Ref. 13). The relative decay of the dipole concentration with anneal time is plotted in Fig. 2. An equilibrium value is still slowly developing after 1600 h of sample annealing. None of the other centers present in the as-grown condition has measurable absorption peaks similar to site a. However, corrections to the line intensity for site a in the $^7F_0 \rightarrow ^5D_0$ excitation spectrum are made from the corresponding absorption measurement to determine the relative growth rate of the cluster sites. Growth curves for the individual sites are obtained by plotting the ratio of the peak areas for the site of interest to site a corrected for dipole decay. The peak areas of site a for subsequent anneal times following the quench are normalized to the peak area corresponding to $t=0$. Figure 3 shows the growth curves for sites g/k, d, and j relative to site a. Site g/k is a rapidly growing cluster, reaching its equilibrium value in just under 100 h. The relative contributions from sites g and k to the rate of the growth curve are determined from the high-resolution $^5D_0 \rightarrow ^7F_1$ fluorescence spectrum for laser excitation corresponding to site g/k in $^5D_0$ (689.85 nm). The fluorescence spectrum consists of a series of well-resolved transitions belonging to both sites as shown in Fig. 4. Line assignments are determined by comparing the same spectrum for different crystal temperatures as described in Ref. 13. Fluorescence lifetimes of the $^5D_0$ level for sites a, k, and g are tabulated for different crystal temperatures to emphasize the severity of fluorescence quenching for site k and site a. Measurement of the $^5D_0 \rightarrow ^7F_1$ fluorescence spectrum for site g/k after each annealing treatment reveals that the transitions retain their relative intensities for all anneal times. Thus both sites form with identical rates suggesting that they belong to the same cluster. A

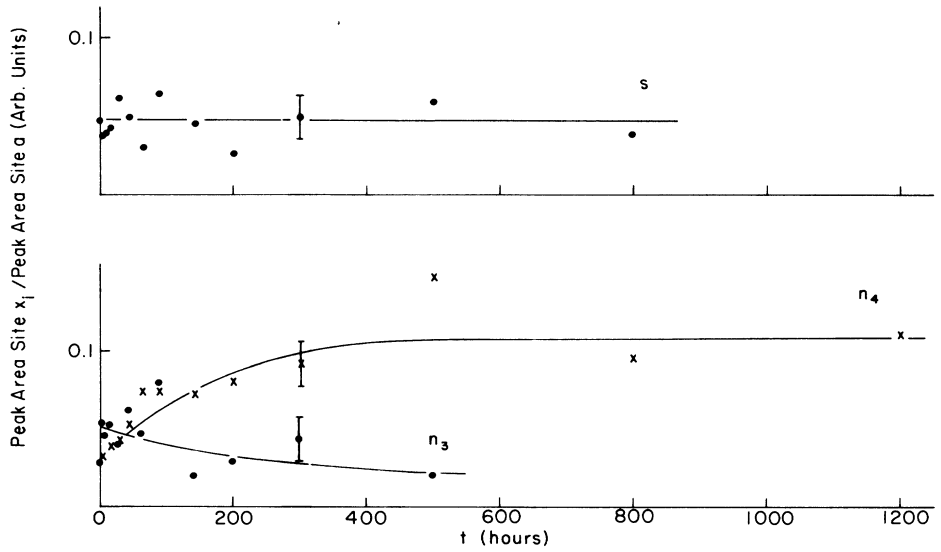

FIG. 5. Growth curves for sites s (690.07 nm), n_4 (690.67 nm), and n_3 (688.41 nm) relative to site a for the 89-ppm crystal annealed at 50 °C. These minor sites appear in the spectrum as a result of the high-temperature quench. The growth curves were determined from excitation spectra measured with a delay of 40 μs and gate of 1 ms. The curves are to guide the eye.

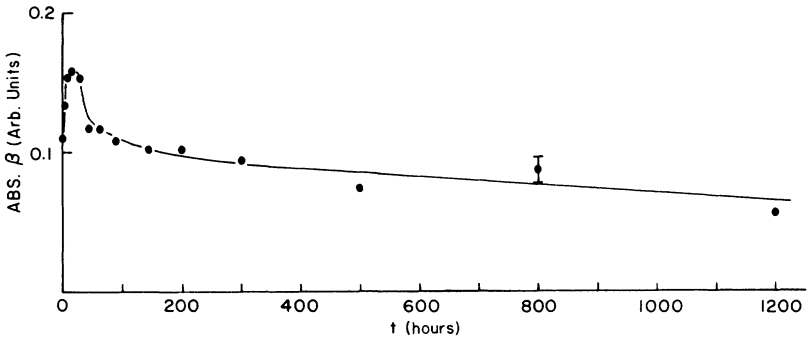

FIG. 6. Absolute changes in site-β concentration (689.31 nm) measured at 637.23 nm in absorption for the 89-ppm crystal annealed at 50 °C. The curve is to guide the eye.

series of high-resolution $^7F_0 \rightarrow {}^5D_0$ excitation spectra obtained by sequentially monitoring fluorescence corresponding to each of the transitions appearing in Fig. 4 shows that sites k and g overlap identically in the $^5D_0$ level.

The growth curve for site d in Fig. 3 closely parallels the behavior exhibited by site g/k since the rate and time taken to reach equilibrium are comparable. Site j, however, has a different growth curve. As seen in Fig. 1, site j was completely eliminated by the high-temperature quench and the growth curve shown in Fig. 3 indicates that it does not begin to reappear until the anneal time exceeds 30 h. Between 300 and 500 h, a discontinuity occurs in the growth curve indicating an abrupt increase in the relative concentration of site j. The excitation spectra corresponding to this region of the curve display a distinct increase in the integrated area accounting for the abrupt rise. As discussed in Ref. 13, site j represents a continuum of sites that have similar spectral characteristics. The temporal behavior displayed by site j (see Fig. 3) suggests the formation of a number of different higher-order clusters. The increase in area would then be the result of additional sites forming in these larger clusters.

The growth curves for three of the four minor sites that appear as a result of the high-temperature quench are shown in Fig. 5 relative to site a. The relative concentrations have been corrected for dipole decay. Their low intensity is reflected by the scatter in the data but the curves indicate that site s and site n_3 show almost no variation in relative concentration with sample annealing. The growth curve for site n_4, on the other hand, appears to behave in a manner similar to sites g/k and d. Site β has a measurable absorption peak at 637.23 nm in the $^5D_1$ region so that absolute changes in site concentration with anneal time could be monitored. The results are plotted in Fig. 6 and show an abrupt rise and decline within the first 100 h followed by a slowly decreasing concentration through 1200 h. The high-resolution $^7F_0 \rightarrow {}^5D_1$ excitation spectrum monitoring fluorescence at 689.20 nm for site β is shown in Fig. 7(a) and the $^5D_0 \rightarrow {}^7F_{0,1}$ fluorescence spectra exciting at 637.23 nm in the $^5D_1$ excitation region appear in Figs. 7(b) and 7(c), respectively. The $^7F_0 \rightarrow {}^5D_1$ excitation spectrum for site β appears identical to the $^7F_0 \rightarrow {}^5D_1$ excitation spectrum for site a, except shifted to longer wavelengths. The arrows in Fig. 7(a) indicate the peak positions of site a for the comparable $^7F_0 \rightarrow {}^5D_1$ excitation spectrum. The fluorescence spectra show a contribution from site a due to the much higher site concentration and the preferential excitation of this site in the $^5D_1$ level. The striking spectral resemblance of site β to site a suggests similar defect symmetries. It is also in-

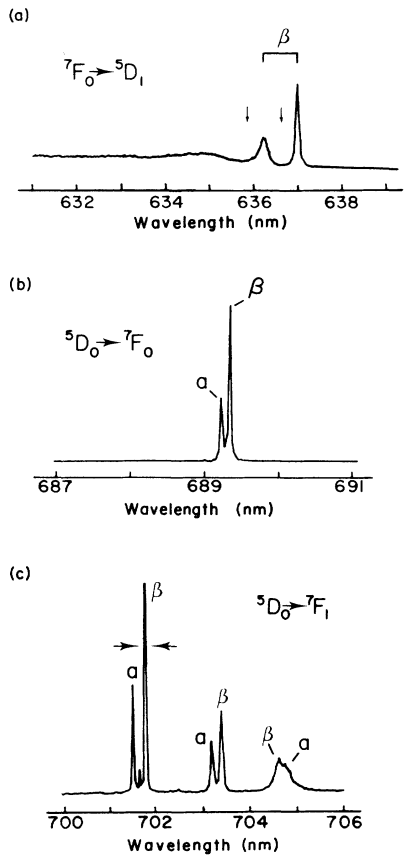

FIG. 7. (a) $^7F_0 \rightarrow {}^5D_1$ excitation spectrum for site β monitoring fluorescence at 689.30 nm. The arrows indicate the relative peak positions of site a for the comparable $^7F_0 \rightarrow {}^5D_1$ excitation spectrum. (b) $^5D_0 \rightarrow {}^5F_0$ fluorescence spectrum exciting the $^5D_1$ level at 637.23 nm. (c) $^5D_0 \rightarrow {}^7F_1$ fluorescence spectrum exciting the $^5D_1$ level at 637.23 nm.

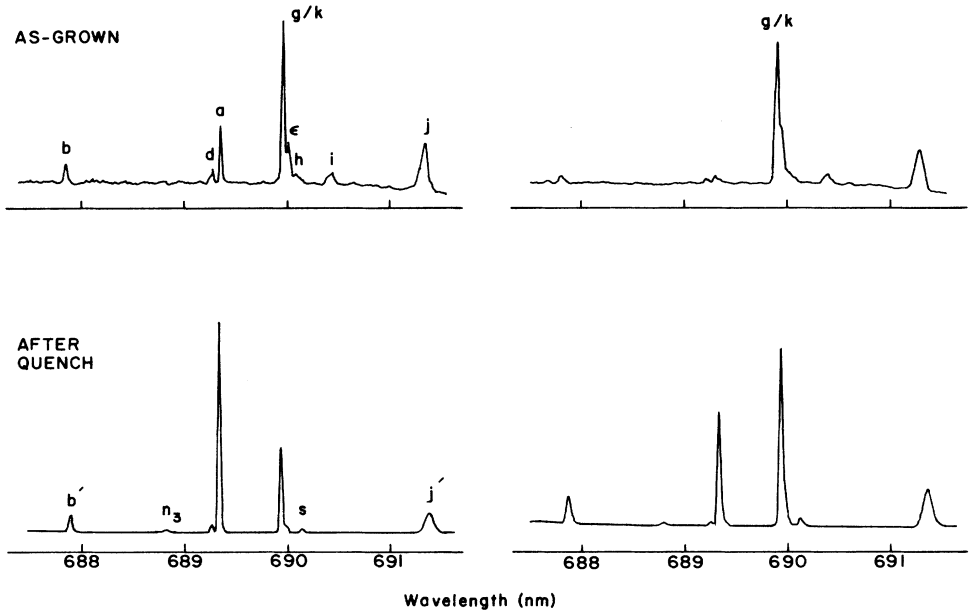

FIG. 8. $^7F_0 \rightarrow {}^5D_0$ excitation spectrum monitoring fluorescence from all sites at 726.5 nm in the 121-ppm crystal. The left column corresponds to a delay of 50 μs and gate of 1 ms; the right column corresponds to a delay of 70 μs and gate of 100 μs. The spectra show the changes in the site distribution that result from the high-temperature anneal-quench procedure.

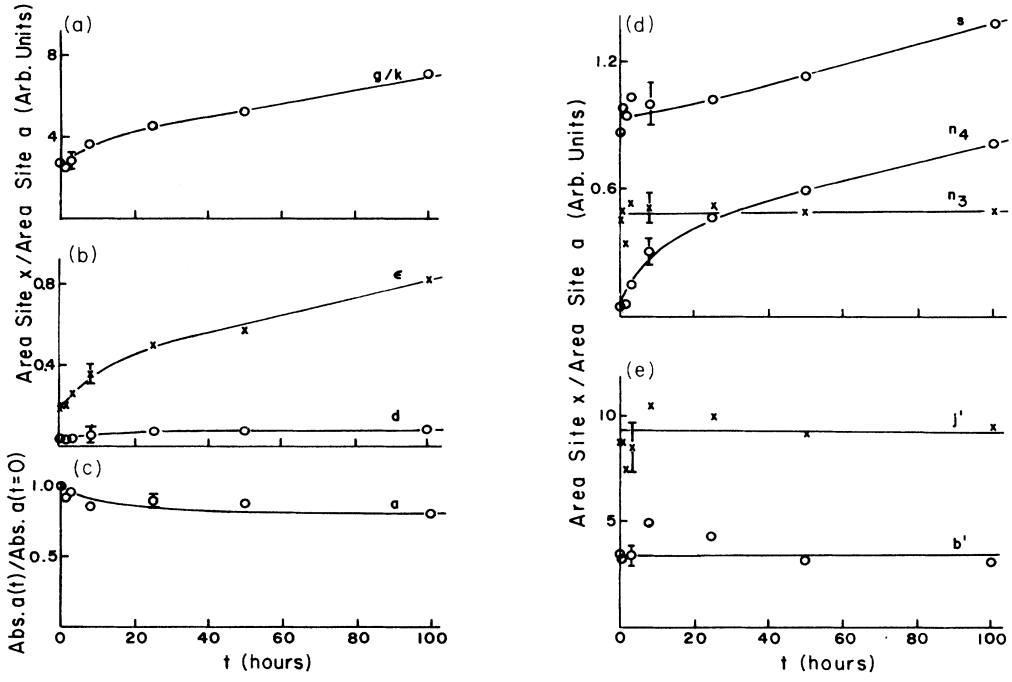

FIG. 9. Changes in site concentration for the 121-ppm crystal annealed at 50°C. (a) Relative fluorescence intensity of site g/k to site a for gated detection with 30-μs delay and 100-μs gate width, respectively. (b) Relative fluorescence intensity of sites ϵ and d to site a for 70-μs delay and 100-μs gate widths. (c) Integrated absorbance of site a. (d) Relative intensity of sites s, n_4, and n_3 to site a for 30-μs delay and 100-μs gate widths. (e) Relative intensity of sites b' and j' to site a for 30-μs delay and 100-μs gate widths. The curves are to guide the eye.

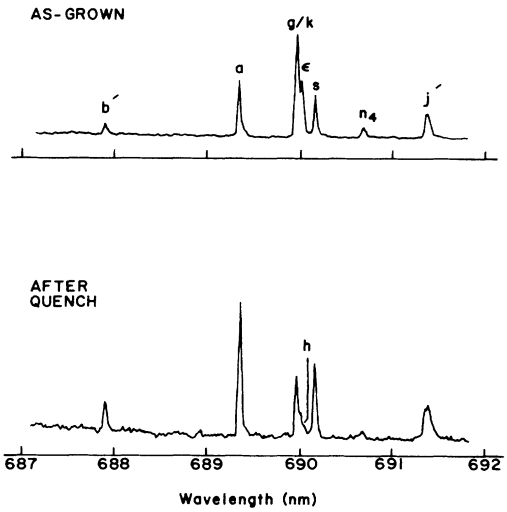

FIG. 10. $^7F_0 \rightarrow {}^5D_0$ excitation spectrum monitoring fluorescence from all sites at 726.5 nm for the 27-ppm crystal. The spectra were collected with a 30-μs delay and 100-μs gate to show the changes in the site distribution that result from the high-temperature anneal-quench procedure.

teresting to note that the rise and decline of the site-β concentration coincides with the same annealing interval required for sites g/k and d to reach equilibrium.

B. Concentration dependence of the site distribution kinetics

The site distribution changes were measured in other concentration samples at 50 °C over a more limited range of annealing times.

Figure 8 shows the changes that occur after the high-temperature anneal-quench procedure for a 121-ppm crystal for gate widths and delay times of 1 ms and 50 μs, respectively, in the left column and 100 and 70 μs in the right column. The latter conditions favor detection of the short-lived sites. The spectra before quenching have the same sites as observed in the 89-ppm crystal (see Fig. 1 for comparison) with the exception of the c site. After quenching, the cluster sites are markedly reduced while the site a concentration (dipoles) increases dramatically. As observed in the 89-ppm crystal, sites n_3 and s weakly appear in the spectrum following the quench. Site n_4 is also detected at the shorter delay times but site β was never observed over the entire annealing period of 100 h. In addition, the positions of the lines associated with sites b and j have shifted slightly and the lifetime of the $^5D_0$ level fluorescence for site b is significantly shortened. The lines are labeled b' and j' to reflect these differences. The site redistribution that occurs after 100 h of annealing at 50 °C for the different sites is shown in Fig. 9. The changes in site a are obtained from the absorption spectrum while the other sites are measured by their relative intensity to site a. Sites n_3, n_4, and s are minor sites whose behavior is similar to the 89-ppm crystal.

Figure 10 shows the spectra for a 27-ppm crystal before and after the annealing-quenching procedure. The minor sites b', j', s, and n_4 observed in the 121-ppm crystal only

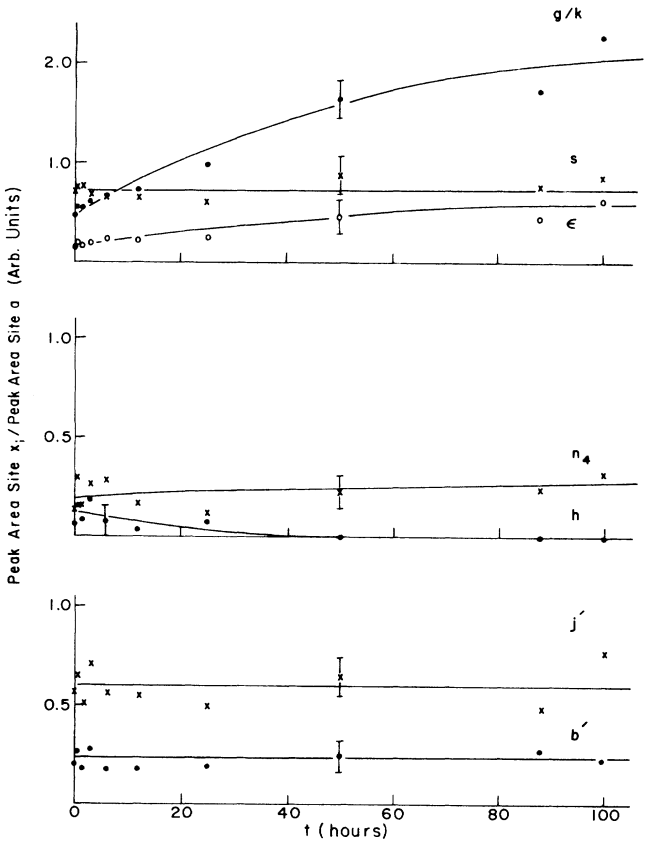

FIG. 11. Growth curves for all measurable sites relative to site a for the 27-ppm crystal annealed at 50 °C. All the growth curves were determined from excitation spectra measured with a delay of 30 μs and gate of 100 μs. The ratios corresponding to the unannealed sample are as follows: site g/k, 1.94; site s, 0.86; site ϵ, 0.84; site n_4, 0.28; site j', 0.75; site b', 0.26. Site h appears in the spectrum as a result of the high-temperature quench. The data for sites h and ϵ are displayed as the ratio of peak heights. The curves are to guide the eye.

after the high-temperature quench are present in the 27-ppm crystal before quenching. Another minor site labeled h appears after the quenching at $\lambda = 689.97$ nm in this crystal. Both sites a and g/k change after the quenching procedure but the other sites remain relatively constant, as can be seen in Fig. 11.

The spectra for an 11-ppm crystal are shown in Fig. 12 before and after the annealing-quenching procedure. Sites b' and j' are particularly strong in the crystal before quenching but the other sites are quite similar to the 27-ppm crystal. After annealing, however, most of the sites are eliminated except sites a and s. A new line labeled n_1 appears that had not been observed in the other samples. The changes that occur when the sample is annealed at 50 °C are shown in Fig. 13. The spectrum of the sample after 50 h of annealing is shown in Fig. 12(c). There is no indication of lines from sites b' and j' at the long annealing times.

The annealing experiments show that there are differences between the minor sites depending on the Sm^{2+}

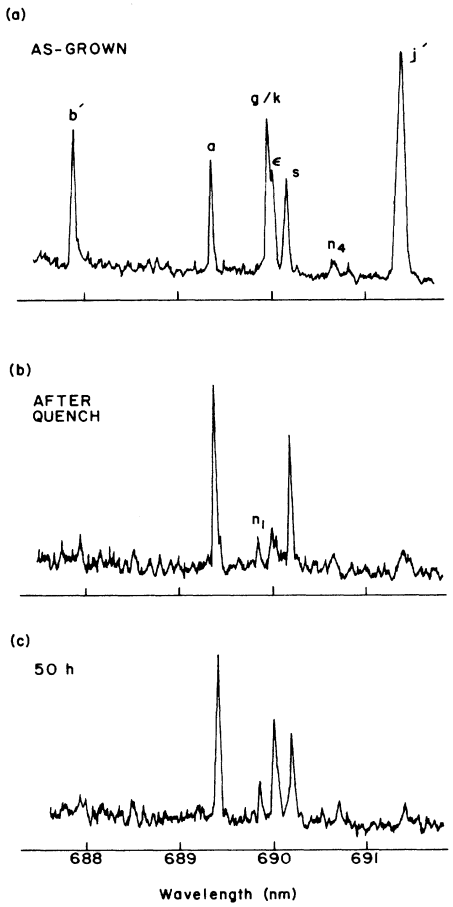

FIG. 12. $^7F_0 \rightarrow {}^5D_0$ excitation spectrum monitoring all fluorescence from all sites at 726.5 nm for the 11-ppm crystal. The spectra were collected with a 30-μs delay and 100-μs gate: (a) unannealed sample, (b) following high-temperature anneal-quench procedure, (c) annealed at 50 °C for 50 h.

concentration and that most of the minor sites do not change during the annealing procedure. The dominant sites in all the crystals are site a and site g/k and it is the behavior of these centers which was studied further. We neglect the contribution from any other site that may become important at longer annealing times. In order to evaluate the kinetics of the site distribution, it is necessary to have absolute concentrations of the two sites. If $n_{\rm tot}$, n_a, and $n_{g/k}$ represent the total dopant concentration and the concentrations of sites a and g/k, respectively, and if in general the concentration of site x is expressed as

$$n_x = \gamma_x I_x \ , \tag{1}$$

where I_x is the excitation line intensity of site x and γ_x is a proportionality constant, then

$$n_{\rm tot} = n_a + \gamma_{g/k} I_{g/k} \ . \tag{2}$$

Since the intensity of site g/k is measured relative to site a in our spectra, we rewrite Eq. (2) as

$$n_{\rm tot} = \left[1 + \frac{\gamma_{g/k}}{\gamma_a} \frac{I_{g/k}}{I_a} \right] n_a \ . \tag{3}$$

Values for $n_{\rm tot}$ and $I_{g/k}/I_a$ can be measured directly, while values proportional to n_a can be measured from the site-a absorption strength during the annealing of the 121-ppm crystal:

$$A_a = \epsilon_a b n_a \ , \tag{4}$$

where A_a, ϵ_a, and b are the integrated absorbance, proportionality constant, and pathlength, respectively. Thus

$$n_{\rm tot} = \left[1 + \frac{\gamma_{g/k}}{\gamma_a} \frac{I_{g/k}}{I_a} \right] \frac{A_a}{\epsilon_a b} \ . \tag{5}$$

Equation (5) was then used in a multiple regression analysis to obtain the best values for $(\gamma_{g/k}/\gamma_a)$ and ϵ_a

TABLE I. The fractional concentrations of site g/k as determined for each of the different concentration crystals. The $n_a/n_{\rm tot}$ ratios determined to give the best value for $\gamma_{g/k}/\gamma_a$ are also included (see text for discussion).

Anneal time (h)	$n_a/n_{\rm tot}$	$(n_{g/k}/n_{\rm tot})_{121\ \rm ppm}$	$(n_{g/k}/n_{\rm tot})_{89\ \rm ppm}$	$(n_{g/k}/n_{\rm tot})_{27\ \rm ppm}$	$(n_{g/k}/n_{\rm tot})_{11\ \rm ppm}$
0	0.820	0.194	0.118	0.040	0.018
0.5	0.815	0.202	0.153	0.046	
1.5	0.805	0.172		0.046	0.024
3	0.792	0.195		0.051	
6				0.056	
8	0.756	0.241	0.205		0.031
12				0.061	
16			0.309		
25	0.691	0.284		0.080	0.036
28			0.329		
44			0.412		
50	0.664	0.314		0.127	0.047
64			0.458		
88			0.508	0.134	
100	0.657	0.426		0.167	0.060

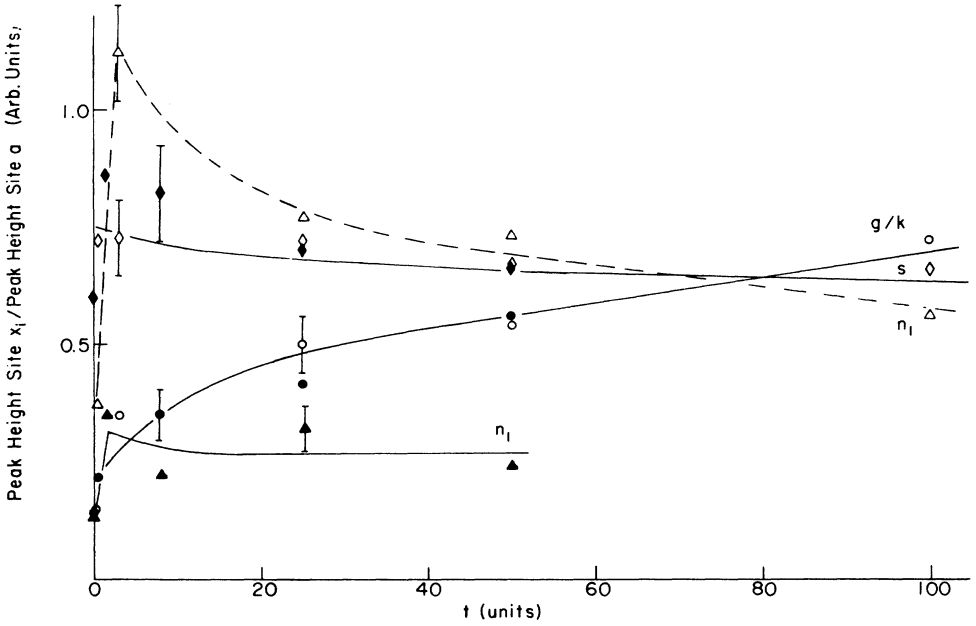

FIG. 13. Growth curves for sites g/k (689.85 nm), s (690.07 nm), and n_1 (689.69 nm) relative to site a for two 11-ppm crystals annealed at 50 °C. Open and closed symbols are used to differentiate the crystals. The growth curves were determined from excitation spectra with a delay of 30 μs and gate of 100 μs. The data are plotted as ratios of peak heights. The ratios corresponding to the unannealed sample for sites g/k and s are 1.06 and 0.66, respectively. Site n_1 appears in the spectrum as a result of the high-temperature quench. The curves are to guide the eye.

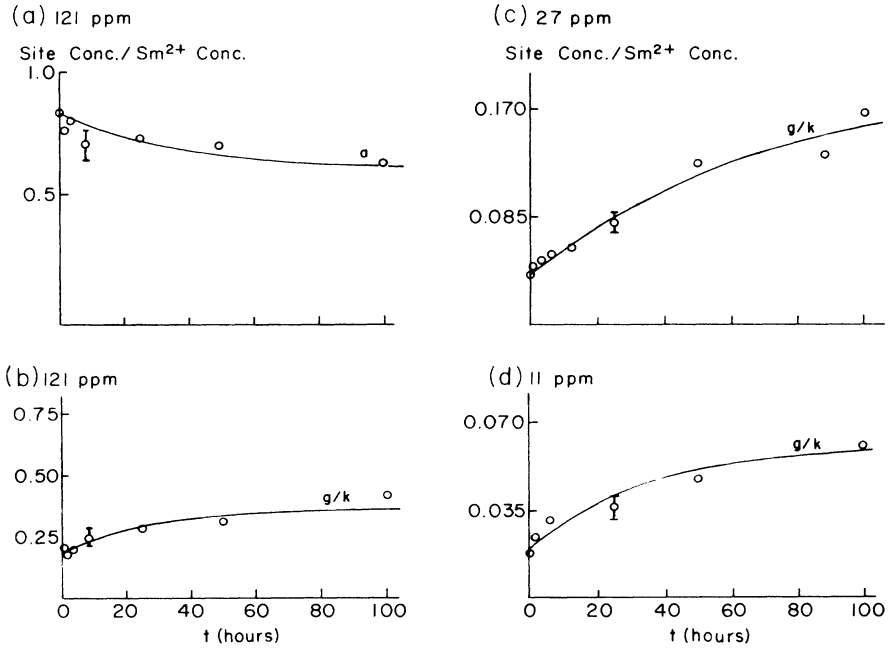

FIG. 14. Fits of the time dependence of the site-a concentration in the 121-ppm crystal (a) and the site g/k concentration in the 121-ppm crystal (b), the 27-ppm crystal (c), and the 11-ppm crystal (d) to Eq. (9). The fits to Eq. (11) are almost identical. The y axis in each figure represents the ratio of the individual site concentration to the total Sm^{2+} concentration.

TABLE II. Values of the adjustable parameters derived from dimer and trimer models with back reaction for site g/k concentration for different initial concentrations.

Crystal concentration (ppm)	Model	p_0/n_{tot}	p_0/n_{tot}	n_{equil}/n_{tot}	Adjustable input parameters C_D (dimer) (h^{-1}) $\left[n_{equil}+\frac{n_{equil}n_{tot}}{(n_{tot}-n_{equil})}\right]k_2$	C_T (trimer) (h^{-1}) $-\left[\frac{n_{equil}^2(3n_{tot}-2n_{equil})}{n_{tot}-n_{equil}}\right]k_3$
121	dimer	0.180		0.630	0.0350	
121	trimer		0.180	0.630		−0.0350
89	dimer	0.12		0.510	0.0300	
89	trimer		0.12	0.510		−0.0300
27	dimer	0.040		0.800	0.0130	
27	trimer		0.040	0.800		−0.0130
11	dimer	0.020		0.940	0.0300	
11	trimer		0.020	0.940		−0.3000

over the entire range of annealing times of the 121-ppm crystal. The data used in the analysis are shown in Figs. 9(a) and 9(c). The resulting values reproduced a constant value for n_{tot} in Eq. (5) over the entire range of annealing conditions. These values for $\gamma_{g/k}/\gamma_a$ were then used to obtain the concentrations of the sites in the other crystals, using the relative intensity measurements of the site-g/k lines to the site-a lines and assuming that only those sites were important during the initial 100-h annealing period. The results are summarized in Table I.

The kinetics for the formation of dimers including back reaction is described by

$$\frac{dn}{dt}=-k_2n^2+k_{-2}p\ , \tag{6}$$

where

$$n+p=n_{tot}\ , \tag{7}$$

while the equation

$$\frac{dn}{dt}=-k_3n^3+k_{-3}q \tag{8}$$

describes the kinetics for the formation of trimers. The concentration of dipoles, dimers, and trimers expressed as fractional concentrations relative to the total impurity concentration is represented by n, p, and q, respectively. The rate constants are represented by k_2 and k_3 for dimers and trimers, respectively. The solutions to these equations have been given by Unger and Perlman[5] and by Rubio and co-workers.[11] For dimer formation,

$$\ln\left[\frac{n/n_{tot}+\frac{1}{(n_{tot}/n_{equil}-1)}}{n/n_{tot}-n_{equil}/n_{tot}}\right]=n_{tot}\left[\frac{n_{equil}}{n_{tot}}+\frac{n_{equil}/n_{tot}}{(1-n_{equil}/n_{tot})}\right]k_2t+C_{initial}\ , \tag{9}$$

where

$$C_{initial}=\ln\left[\frac{(1-p_0/n_{tot})+\frac{n_{equil}/n_{tot}}{1-n_{equil}/n_{tot}}}{(1-p_0/n_{tot})-n_{equil}/n_{tot}}\right]\ , \tag{10}$$

and for trimer formation,

$$\ln\left[\frac{n}{n_{tot}}-\frac{n_{equil}}{n_{tot}}\right]=n_{tot}^2\left[\frac{-3(n_{equil}/n_{tot})^2+2(n_{equil}/n_{tot})^3}{(1-n_{equil}/n_{tot})}\right]k_3t+C_{initial}\ , \tag{11}$$

TABLE III. Values of the rate constants derived from the dimer model with back reaction for site g/k concentration versus annealing temperature. Crystal concentration is 95±6 ppm.

Annealing temperature (°C)	$10^{-3}T^{-1}$	p_0	n_{equil}/n_{tot}	k_2 ([(mole fraction) h]$^{-1}$)
40	3.195	0.130	0.560	75
50	3.096	0.120	0.510	410
70	2.9155	0.130	0.510	680

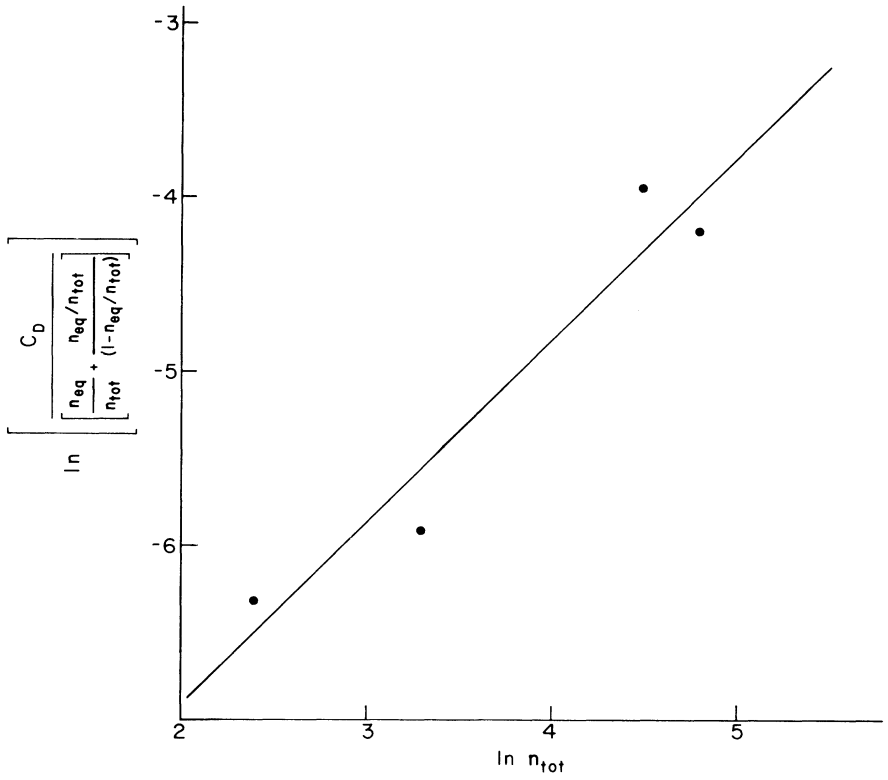

FIG. 15. Plot of $\ln\{C_D/[n_{\text{equil}}/n_{\text{tot}}+(n_{\text{equil}}/n_{\text{tot}})/(1-n_{\text{equil}}/n_{\text{tot}})]\}$ versus $\ln n_{\text{tot}}$. The C_D and $n_{\text{equil}}/n_{\text{tot}}$ values were obtained from the fits of the fractional growth of site g/k relative to n_{tot} to pure second-order kinetics including back reaction (see text). The slope of the line is 1.04 ± 0.21, in agreement with a second-order reaction.

where

$$C_{\text{initial}}=\ln\left[1-\frac{q_0}{n_{\text{tot}}}-\frac{n_{\text{equil}}}{n_{\text{tot}}}\right]. \tag{12}$$

Here n_{equil} corresponds to the equilibrium concentration of dipoles and p_0 and q_0 are the initial concentrations of ions in dimer and trimer sites, respectively, at $t=0$ since there is an appreciable concentration at the beginning of the annealing. Both expressions fit the observed data equally well as has been pointed out previously.[9–12] Typical fits are shown in Figs. 14(b) and 14(c) for site g/k in the three different concentration crystals, assuming that the defect corresponds to either sites in a dimer or a trimer, and in Fig. 14(a) for site a in the highest concentration crystal where the decrease can be accurately measured by absorption spectroscopy. The fits are essentially identical for second- or third-order kinetics. Table II lists the values for the coefficients of t, labeled C_D and C_T, respectively, and $n_{\text{equil}}/n_{\text{tot}}$ in Eqs. (9) and (11).

TABLE IV. Comparison of activation energies for similar divalent impurities in KCl.

System	E_a (eV)	Reference
KCl:Sm^{2+}	0.63	This work
KCl:Sr^{2+}	0.73	2
KCl:Eu^{2+}	0.86	17
KCl:Eu^{2+}	0.86	11

The order of the kinetics can be distinguished on the basis of the concentration dependences of C_D or C_T. From Eqs. (9) and (11), their value depends either linearly or quadratically on n_{tot}. The actual dependence can be determined by a least-squares fit to the equations

$$\ln\left[\frac{C_D}{\left[\frac{n_{\text{equil}}}{n_{\text{tot}}}+\frac{n_{\text{equil}}/n_{\text{tot}}}{(1-n_{\text{equil}}/n_{\text{tot}})}\right]}\right]=\ln n_{\text{tot}}+\ln k_2\,, \tag{13}$$

$$\ln\left[\frac{C_T}{\left[\frac{-3(n_{\text{equil}}/n_{\text{tot}})^2+2(n_{\text{equil}}/n_{\text{tot}})^3}{(1-n_{\text{equil}}/n_{\text{tot}})}\right]}\right]=2\ln n_{\text{tot}}+\ln k_3\,, \tag{14}$$

using the n_{equil}/n_{tot} and C_D or C_T values in Table II. The fit shown in Fig. 15 for Eq. (13) yields a slope of 1.04 ± 0.21 and a correlation coefficient of 0.96. A similar fit for Eq. (14) yields a slope of 1.17 ± 0.26 and a correlation coefficient of 0.95. The slope is in agreement with that expected for secon order kinetics and site g/k is shown to be the dimer th : forms initially during aggregation.

C. Activation energy for dimer formation

An activation energy for the formation of the g/k dimer can be determined from an Arrhenius plot of $\ln k_2$ versus $1/T$ since $k_2=\nu_0\exp(-E_A/kT)$. The growth curves for site g/k in cry: ils with the same impurity content must therefore be dd-ermined at different annealing temperatures. Differen[at]s in the growth rates were measured at 40, 50, and 70 : for three crystals with an average dopant concentratic.. of 95 ± 6 ppm. Annealing temperatures corresponding to 110 and 200 °C were also selected, but these temperatures appear too high to allow aggregation of the dipoles. For the sample annealed at 110 °C, site g/k was observed to undergo a modest increase of approximately 1.5 times relative to site a for the first 90 min of annealing but showed no further growth over a total anneal time of 500 h. The crystal annealed at 200 °C showed no change in the intensity of the site g/k transition relative to site a over a total anneal time of 143 h.

The growth curves were fit to the dimer model with back reaction as described in the preceding section. The values of the adjustable parameters used to fit the temperature data are tabulated in Table III. The Arrhenius plot is obtained from the values shown for k_2. The activation energy calculated from the slope of the least-squares fit to the data is 0.63 ± 0.28 eV, a value that is consistent with previously reported values in similar systems.[2,11,17] A comparison between the different values is given in Table IV. The preexponential factor is determined from the y intercept to have a value of 1.5×10^{12} s^{-1}, in good agreement with a previously published value of 4×10^{13} s^{-1} for KCl:Sr^{2+}.[2]

IV. CONCLUSIONS

The method of site-selective laser spectroscopy has been applied to the study of the aggregation kinetics of $(Sm_K\cdot V_K)^x$ dipoles in KCl. Unlike previous studies, these experiments represent the first detailed investigation of the aggregation products. The $^7F_0\rightarrow{}^5D_0$ excitation spectrum reveals that site g/k is the dominant cluster site. This site is also observed to undergo marked changes in concentration with anneal time. The other cluster sites are either too low in concentration to be of major influence in the aggregation kinetics during the annealing or do not exhibit large enough changes in their site concentration with sample annealing to account for the dipole decay. The growth curves were fit to dimer and trimer models including the back reaction, and the concentration dependence of the resulting rate constant for site g/k was determined in order to evaluate the reaction order. It was determined that the g/k cluster reappears in the spectrum in a manner consistent with second-order kinetics. As reported earlier, the spectrum of sites g and k overlap identically in the $^7F_0\rightarrow{}^5D_0$ and the weaker $^7F_0\rightarrow{}^5D_1$ excitation regions.[13] High-resolution $^5D_0\rightarrow{}^7F_1$ fluorescence spectra resulting from laser excitation corresponding to the $^7F_0\rightarrow{}^5D_0$ transition for site g/k reveal that both sites grow in with similar rates. The overlapping excitation lines and equal growth rates suggest that the two sites are in fact the two ions that form the dimer itself and that the two sites in the dimer are crystallographically inequivalent since the crystal-field splittings of site g and site k are different. The two nearest-neighbor (nn) dimers proposed in Figs. 1(c) and 1(d) in Ref. 18 are both consistent with the observation of crystallographically inequivalent ions in the dimer, while the simpler nearest-neighbor and next-nearest-neighbor dimers in Figs. 1(a) and 1(d) are not consistent.

The studies also show that the dimer is not the thermodynamically favored site since site j continues to grow at much longer annealing times than those studied here. Larger clusters are expected to form as other phases develop in the lattice. Thus site j may correspond to trimers that have been predicted to be the most stable sites[18] or higher-order clusters. Studies of these latter stages of aggregation will be reported at a future time.

ACKNOWLEDGMENT

This work was supported by the Solid State Chemistry Program of the National Science Foundation under Grant No. DMR-85-13705.

*Present address: Lawrence Livermore National Laboratory, Livermore, CA.

[1]J. S. Cook and J. S. Dryden, Austr. J. Phys. **13**, 260 (1960).
[2]J. C. Cook and J. S. Dryden, Proc. Phys. Soc. (London) **80**, 479 (1962).
[3]S. L. Naberhuis and F. K. Fong, J. Chem. Phys. **56**, 1174 (1972).
[4]J. H. Crawford, Jr., J. Phys. Chem. Solids **31**, 399 (1970).
[5]S. Unger and M. M. Perlman, Phys. Rev. B **10**, 3692 (1974).
[6]J. S. Cook and J. S. Dryden, Phys. Rev. B **12**, 5997 (1975).
[7]S. Unger and M. M. Perlman, Phys. Rev. B **12**, 5997 (1975).
[8]G. J. Dienes, Semicond. Insul. **4**, 159 (1978).
[9]E. Lilley, J. Phys. (Paris) Colloq. **41**, C6-429 (1980).
[10]J. E. Strutt and E. Lilley, Phys. Status Solidi A **33**, 229 (1976).
[11]A. Muñoz F., E. Carbrera, B., H. Riveros, R., M. Patron, and J. Rubio O., Phys. Rev. B **31**, 8196 (1985).
[12]A. Muñoz F., A. Galo, M. Patron, and J. Rubic O., Phys. Rev. B **32**, 8408 (1985).
[13]A. J. Ramponi and J. C. Wright, Phys. Rev. B **31**, 3965 (1985).

[14]M. P. Miller, D. R. Tallant, F. J. Gustafson, and J. C. Wright, Anal. Chem. **49**, 1474 (1977).

[15]Two of the crystals were grown by Dr. Joel Martin and Mr. Charles Hunt from the Oklahoma State University Crystal Growing Facility, Stillwater, OK 74078. The other crystals were graciously provided by Dr. F. K. Fong and Dr. R. H. Heist.

[16]K. Suzuki, J. Phys. Soc. Jpn. **16**, 67 (1961).

[17]S. Unger and M. M. Perlman, Phys. Rev.B **6**, 3973 (1972).

[18]J. Corish, J. M. Quigley, C. R. A. Catlow, and P. W. M. Jacobs, J. Phys. (Paris) Colloq. **41**, C6-68 (1982).